Measurements by MRI of the Settling and Packing of Solid Particles from Aqueous Suspensions

Julio Acosta-Cabronero and Laurance D. Hall
Herchel Smith Laboratory for Medicinal Chemistry, University of Cambridge School of Clinical Medicine, Cambridge, CB2 2PZ, U.K.

DOI 10.1002/aic.11754
Published online April 27, 2009 in Wiley InterScience (www.interscience.wiley.com).

This study extends the application of existing magnetic resonance imaging methods to measure the settling of solid particles from aqueous suspensions. The acquisition of one-dimensional multiecho projections allowed the direct measurement of initial magnetizations (M_0), from which solid volume fractions along the sedimentation column were inferred. For polystyrene beads, it was found that monoexponential curves accurately fitted the transverse relaxation decays. In contrast, for the other four solids investigated (activated carbon, talc, calcium carbonate, and glass beads), the single exponential model did not suffice and additional terms in the fitting function significantly improved the calculation of solid concentrations. Additional information about particle sizes was obtained by comparing volume fractions with the spin–spin relaxation times of the hydrogen protons as a function of the vertical height through the sedimenting suspensions of activated carbon and polystyrene beads. © 2009 American Institute of Chemical Engineers *AIChE J, 55: 1426–1433, 2009*
Keywords: settling/sedimentation, suspensions, solid/liquid separations, separation techniques

Introduction

Flotation and sedimentation of particle suspensions continue to be of importance to a wide range of industries. Consequently, methods that can provide accurate measurements of settling/flotation rates and sediment growth, and quantitate the description of interface broadening and sediment packing are increasingly required for optimization of equipment design and its performance. It is already well known that magnetic resonance imaging (MRI) can be used for quantitative measurements of the settling and flotation of monodisperse and polydisperse suspensions of noncolloidal particles.[1–7] Such MRI studies directly provide experimental data that allow the quantitative description of the hindered settling/flotation function, the relative quartile thickness, and the diffusion coefficient, and thereby enable measurements of the contribution that hindered settling, polydispersity, and self-induced hydrodynamic diffusion each make to the sedimentation process.[8]

Most of the existing MRI methods use data obtained from a standard one-dimensional (1D), spin-echo[9] (SE) pulse sequence, which are interpreted on the basis of two assumptions. First, that the volume fraction occupied by particles is proportional to the MR signal intensity from the suspension normalized to that from the sedimenting fluid only. This assumes that the spin-lattice and spin–spin relaxation times (T_1 and T_2, respectively) are independent of the height along the vertical axis of the settled suspension. Second, that in systems for which the spin–spin relaxation time (T_2) is found to depend on the particle volume fraction, it is necessary to use the initial magnetization (M_0) obtained from the relaxation decay assuming a monoexponential curve. Although the

Additional Supporting Information may be found in the online version of this article.

Correspondence concerning this article should be addressed to J. Acosta-Cabronero at this current address: Wolfson Brain Imaging Centre, Addenbrooke's Hospital (Box 65), Hills Road, Cambridge, CB2 0QQ, U.K.; jac@cantab.net

refocusing pulse used in SE measurements eliminates the reversible signal loss because of static magnetic field inhomogeneities, the relative motion between particles and fluid results in a random magnetic field fluctuation, which yields an irreversible loss of phase coherence. For this reason, in some cases the nuclear relaxation curves from the fluids in particulate regions cannot be described by a monoexponential model, which is only valid for sedimenting suspensions that have small local field distortions because of particle size, packing density, and magnetic susceptibility difference between the fluid and solid phases.[10,11]

The purpose of this study is to provide insight to the benefits of using a biexponential model to quantitate the relaxation decay of the MRI responses from the proton resonances of the suspending fluid. A series of examples from both the settling and the subsequent sediment compaction of both colloidal and noncolloidal particles are used to illustrate the need for this more comprehensive method to calculate the particle volume fraction (Φ). In addition, analysis of the two relaxation times (T_{21} and T_{22}) obtained via this method provides further information about the composition of the particulate regions and the behavior of the fluid phase.

Volume fraction calculation

The method used here to calculate the local particle concentrations is essentially that of Turney et al.,[2,3] where the volume fraction (Φ) as a function of height (h) and time (t) for a suspension is given by:

$$\Phi(h,t) = 1 - \frac{X_{\text{susp}}(h,t)}{X_{\text{ref}}(h,t)}, \tag{1}$$

where X_{susp} and X_{ref} represent either the MRI signal intensity or the initial magnetization (M_0) for the suspension and the reference sample, respectively, along the height of the vertical axis of the container. Turney et al.[2] originally found that the spin-lattice and spin–spin relaxation times were constant through the height of a settled suspension of noncolloidal polystyrene beads and, hence, they used signal intensities as a measure of particle volume fractions. A subsequent publication[2] introduced the use of M_0-values from monoexponential analyses to calculate volume fractions to correct for spin–spin relaxation effects to measure the settling of rod-like particle suspensions.

This study demonstrates that particle volume fractions can be calculated more accurately using the total initial magnetization, $M_0 = M_{01} + M_{02}$, obtained from the best biexponential fit:

$$S(t) = M_{01}e^{-t/T_{21}} + M_{02}e^{-t/T_{22}}, \tag{2}$$

where T_{21} and T_{22} are the spin–spin relaxation times of the suspending fluid.

Experimental

Materials

Five different dry particles were used as representative models for industrial suspensions. Particle density was calculated from the measured weight of the dry particles and the measured weight of a known volume, determined by an 'E-MIL'boro 25 ± 0.03 ml volumetric flask (Fisher Scientific U.K., Loughborough, U.K.), of the particle-in-water solution. Particle size ranges were estimated by measuring the longest diameter of 180–200 particles. Micrographs of the particles were taken with the aid of a digital camera Nikon Coolpix 995 (Nikon Corporation, Tokyo, Japan) attached to a standard inspection microscope Nikon Optiphot 150 (Nikon Corporation, Tokyo, Japan). The open-source software, Gimp (GNU Image Manipulation Program) was used to perform such tasks as measuring distances, editing text layers, cropping images, and converting image formats. The description of the particles is as follows:

- High-purity activated carbon (Darco G-60, Sigma-Aldrich Co., Dorset, U.K.). Particle size range 0.27*–147 μm and density (ρ) 1.2 g cm^{-3}.
- Calcium carbonate ($CaCO_3$), 98% (Sigma-Aldrich Co., Dorset, U.K.). Particle size range 0.12*–7 μm, $\rho = 2.93$ g cm^{-3}.
- Hydrous magnesium silicate (Talc, Sigma-Aldrich Co., Dorset, U.K.). Particle size 0.27*–20 μm, $\rho = 2.75$ g cm^{-3}.
- Polystyrene beads (Polysciences, Warrington, PA), 3- to 17-μm diameter, $\rho = 1.05$ g cm^{-3}.
- Glass beads designed for gas-liquid chromatography (BDH Chemicals, Poole, U.K.). Particle size range 80–148 μm, $\rho = 2.8$ g cm^{-3}. These were soaked overnight in laboratory detergent, then rinsed with several changes of deionized water and, finally, the beads were dried in an oven at 70°C; this cleaning process was repeated twice.

The particle surfaces could be modified to suppress aggregation by addition of low concentrations (0.03% w/w) of a nonanionic surfactant (Triton X-100, BDH Chemicals, Poole, U.K.).

The suspending fluids used for these measurements were either aqueous copper (II) sulfate ($CuSO_4$) solutions (6–14 mM) or blends of 98% glycerol (RECTAPUR, Merck & Co., NJ) with deionized water. The paramagnetic relaxation reagent, $CuSO_4$, was added to the liquid phase to avoid impractical scan times.

Equipment

All MRI experiments were performed using a 4.7-T Bruker PharmaScan MRI system: 160-mm diameter horizontal bore, actively screened magnet (Magnex Scientific, Oxford, U.K.), interfaced with a Bruker PharmaScan console operating with Paravision 2.1.1 software (Bruker Medizin Technik GmbH, Karlsruhe, Germany). The 90-mm diameter self-shielded and water-cooled Bruker gradient set has a maximum gradient strength of 293 mT/m. The Bruker r.f. probe was a 61-mm internal diameter, 100-mm length quadrature birdcage coil tuned and matched to the hydrogen (^{1}H) nuclear frequency of 200.21 MHz.

Imaging protocol

The imaging protocol used to acquire nonslice selective, 1D MRI images of the sedimenting suspensions was a standard Carr-Purcell-Melboom-Gill[12] (CPMG) sequence (i.e., in the absence of phase and slice-encoding gradients). Each 1D projection was the average of two echo-trains, each

*The lower bound is limited by the micrograph resolution.

consisting of 60 equally spaced echoes. The minimum inter-echo time allowed by hermite r.f. pulses (2000 and 1240 μs in duration, respectively) was 5.93 ms. It is important to note that although the use of two soft hermite pulses induces a strong time penalty to the echo acquisition, it was found empirically that, because of the quality of the B_1 field, the decay of the echo-train for hermite pulses was cleaner compared to that generated by hard block pulses using ParaVision 2.1.1. The time between the excitation pulse of each echo-train was 1353 ms, and 128 data points were acquired for each echo giving a linear resolution of 141 μm from a field of view (FoV) of 18 mm.

Temperature control

Suspensions were prepared 2 h before each sedimentation measurement; two glass vessels (internal diameter 2 cm, and length 3 cm), one containing the sedimenting suspension and the other the pure suspending fluid, were kept at reduced pressure to extract air bubbles, and then allowed to achieve thermal equilibrium in the bore of the magnet.

In situ temperature measurements at the centre of the water-cooled gradient set in the magnet's bore were made using a fiber optic thermometry system (ORS model, Fiso Technologies, Quebec, Canada). Temperature stability was 17.01°C $\pm$ 0.02°C over a period of 2 h during an imaging experiment.

Setup and reference scan

Flat-bottomed cylindrical acrylic vials (internal diameter 1 cm and length 1 cm) were used for all MRI measurements; all tubes were carefully washed before use.

A suspending fluid reference sample fixed on a Perspex platform was accurately placed at the centre of the imaging region before each measurement by sliding the assembly into the r.f. probe on a Perspex rail. The transmit coil was then tuned and matched, and its resonant frequency and the shimming of the magnetic field homogeneity both optimized. Subsequently, the excitation and refocusing r.f. pulses were calibrated, and the receiver gain adjusted so that the digitizer filling was below 66%.

A reference scan, which was a single 1D projection, was used to normalize the sedimentation profiles as described in Eq. 1. This normalization is necessary to correct for spatially dependent signal variations usually attributed to poor radio-frequency field (B_1) homogeneity or gradient-driven eddy currents.

Suspension scan

The scan parameters used for the reference sample were then copied, and the pulse sequence was looped to sample the time evolution of the settling process plus the sediment packing. The mixture was brought to initial conditions before each MRI measurement by carefully stirring (without creating air bubbles) with a thin needle, until the suspension was dispersed. A sample of the suspension was then extracted with a hypodermic syringe and deposited in the acrylic tube, which was immediately placed at the centre of the probe and the MRI scan started. For samples with high settling rates, the protocol was started in advance to capture the first stages of the process as the sample was slid into the probe.

Measurement accuracy and reproducibility

The aforementioned method introduces some experimental errors, which add to the signal fluctuations intrinsic to the MRI system and can have a critical impact. Because identical positioning of the reference sample and of the suspension is essential in terms of projection coregistration, shimming effectiveness, and possible boundary effects, this was evaluated using two reference samples. This verified that both samples were located within the pixel resolution range, and that the coefficient of variance of the signal was $\sim$0.2% in a pixel-by-pixel basis. Although measured volume fractions in the pure fluid regions studied in this article have a maximum accuracy of 0.01, the uncertainty in the measured concentrations in particulate regions depends on voidage and the magnetic susceptibility difference between the solid and the liquid phase. Both low proton densities and fast MR-signal decays restrict the accuracy of the initial magnetization measurements in the voxels under study.

It was of concern that the mechanical impact due to each gradient pulse could move the position of the sample or induce variations in the settling rate of the suspension. Consequently, measurements were made of the settling of 50% v/v talc in a 0.3–99.7% TRITON X-100–aqueous 8.5 mM $CuSO_4$ solution, to measure the effect that the number of acquired echoes (NE) and the repetition time (TR) of the pulse sequence have on the mechanical shaking and hence on the sedimentation rate. The scan protocol described previously was used for the same suspension sample with three different combinations of TR/NE (500 ms/60, 1353 ms/60, and 100,000 ms/1) for the same suspension. No evidence was found for any motion effect or difference in settling velocities caused by the imaging protocol used in this study.

Data analysis

Fitting algorithm. A multiestimate fitting algorithm based on the Nelder-Mead simplex search method[13] was developed in Matlab (The MathWorks, Natick, MA) to optimize the calculation of multiexponential curves that fit MRI signal decays. This fitting method is based on the hypothesis that the best description of a set of data is one that minimizes the weighted sum of the squares of the deviation of the data from the fitting function. The noise limit was set to a signal-to-noise ratio (SNR) of 7[14]; data points lying below this threshold were not considered for the subsequent fitting to ensure that the background noise did not contribute more than 1% to the calculations.

The validation of the fitting technique illustrated in Table 1 revealed that this algorithm could be used to measure complex exponential decays; however, this study is intentionally restricted to a maximum number of four variables (two exponential terms).

F-test. Although it is intuitively obvious that for many systems a biexponential model may describe the MR-signal decay from either a suspension in, or a sediment of, particles from a fluid more accurately than a single exponential analysis, intercomparisons based on a simple variance of the fit test (χ^2)[15] are traditionally rather uncertain. Hence, for this study, it was decided to use an F-test[15] to compare the numerical results and, thereby, to evaluate whether, or not, the

Table 1. Best Fitting Parameters for 80 Simulated Decay Exponential Data Points with T_2 Components Clustered Around T_{2c1} = 106 ms and T_{2c2} = 20 ms

Exponential Fitting	M_{01} (10^8)	T_{21} (ms)	M_{02} (10^8)	T_{22} (ms)	M_{03} (10^8)	T_{23} (ms)	χ^2 (10^{-14})
Mono-	2.3	71.6	–	–	–	–	43
Bi-	1.4	106	1.5	20	–	–	1.9
Tri-	1.4	91.3	1.4	18.1	0.1	198.2	1.7

addition of new analytical components provides a more accurate description of the experimental data. In practice, two different methods of determining χ^2 were assessed, and the distribution of F_{12} calculated from:

$$F_{12} = \frac{\chi_1^2/\nu_1}{\chi_2^2/\nu_2}, \tag{3}$$

where $\nu_i = NE_i - p_i$ is the number of degrees of freedom corresponding to χ_i^2; that is, the number of echoes over the noise limit (NE) minus the number of variables (p) to be optimized by the method ($p = 2$ for monoexponential fitting and $p = 4$ for biexponential fitting). By comparing the results of F_{12} with critical values from the F-distribution tables[15] ($F > F_{12} > 1/F$), the significance and limits of the added terms can be evaluated.

The values of the F-distribution depend on the probability that the calculation yields a particular value of F_{12}. It was empirically found that values of F for F_{12} less than 1% probable effectively delimit the biexponential signal behavior of the sediment regions analyzed in this study.

Results and Discussion

The first comparative evaluation of the methods summarized earlier used the experimental data obtained from the settling of 15% by volume of activated charcoal, suspended in aqueous $CuSO_4$ (6.3 mM), which took 7′15″ to completion. The signal decay of two voxels, one from the fluid and the other from the sediment region, respectively, was extracted from a 1D projection measured 40 min after the settling was initiated.

Figure 1 shows the measured signal data from both those voxels, plus both the mono- and biexponential curves that best fit those data. It is conclusive from Figure 1a that both models consistently fit the signal decay data from the clear fluid region (monoexponential function parameters: $M_0 = 2.85 \cdot \times 10^5$, $T_2 = 164.8$ ms; biexponential function parameters: $M_{01} = 2.85 \cdot \times 10^5$, $M_{02} = 179$, $T_{21} = 164.7$ ms, $T_{22} = 0.3$ ms). Clearly, the contribution from the second term of the biexponential function to the signal intensity is not significant; the ratio (M_{02}/M_{01}) of the initial magnetization of the two components is $6.3 \cdot \times 10^{-4}$. This indicates that the frequency offset and/or molecular displacement are very small, thus influence of the echo time is negligible.

In contrast, it is clear from the data shown in Figure 1b for the suspension that although the monoexponential fitting function does not accurately describe the signal decay, a two-component analysis does model the signal decay of the voxel from the settled region. Specifically, the function parameters from the monoexponential fitting were $M_0 = 1.23 \cdot \times 10^5$ and $T_2 = 14.9$ ms, and those from the biexponential analysis were $M_{01} = 1.26 \cdot \times 10^5$, $M_{02} = 2.89 \cdot \times 10^4$, $T_{21} = 8.4$ ms, and $T_{22} = 37.7$ ms. It is noteworthy that the contribution from the second term of the initial magnetization is much stronger than in the fluid-only example ($M_{02}/M_{01} = 0.23$). In the sediment voxel, the solid phase causes the fluid protons to precess at a larger range of rates during the interpulse period, and therefore the transverse magnetization presents a fast initial decay followed by a smoother evolution, which is effectively defined by a biexponential curve.

The significance of the different relaxometry components depends on solid concentration and magnetic susceptibility differences in particulate regions. If they are reasonably low, it is easy to justify that one component represents the signal decay from suspending fluid and the other, the faster decay from ''bound'' fluid induced by solid/fluid susceptibility

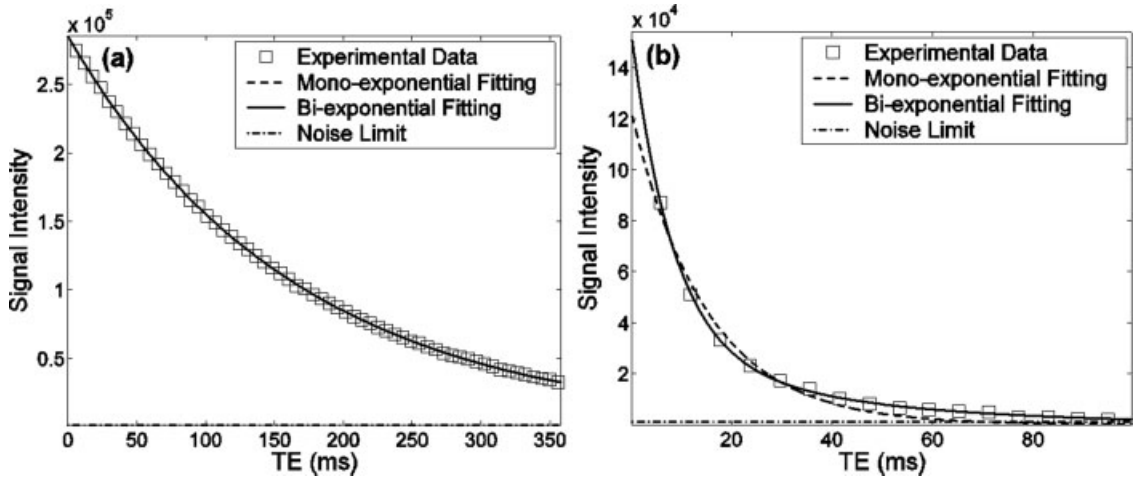

Figure 1. The curves in both graphs represent the mono- and biexponential curves which best fit the signal decay data from the 1D CPMG projection of the height of a settled suspension of 15% v/v activated carbon from aqueous 6.3 mM CuSO4 solution for a single pixel from (a) the pure fluid and (b) the sediment.

Noise limit was set to an SNR of 7 14; data points lying below this limit were not considered for the fitting. For the fluid region (a), all 60 echoes were fitted; for the sediment voxel (b), 23 data points had SNR > 7.

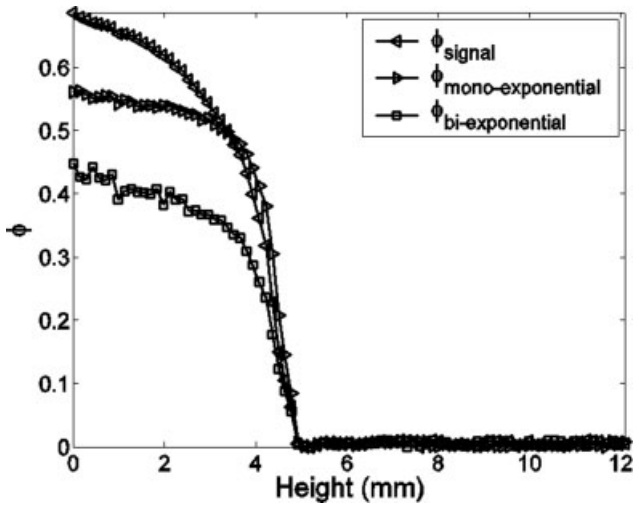

Figure 2. Comparison of particle volume fraction profiles along the height of 15% by vol. activated carbon settled in an aqueous 6.3 mM CuSO4 solution.

The curves shown were calculated from (a) MRI signal intensity, (b) M_0 obtained from the monoexponential curve fitted to signal decay data, and (c) $M_0 = M_{01} + M_{02}$ for the biexponential model.

differences. However, if the concentration and/or susceptibility differences are high, then more than two components may be needed to fully explain the decay. Hence, the biexponential model would just be an approximation, where the two components would average multiple transverse relaxation behaviors. In the case of the charcoal sediment, it is clear that the field distortion caused by magnetic susceptibility differences does not allow a clear bound-/free-fluid signal behavior separation, and the two components are highly driven by the large range of precession rates.

Figure 2 compares the vertical volume fraction profiles of the settled suspension calculated by the three methods described earlier. It is apparent from this comparison that the estimated particle volume fractions are systematically higher in the sediment region for the monoexponential and first-echo methods. It is also evident that the packing density gradient typical for compressible sediments of colloidal particles follows different patterns for each of the three methods. Particularly, an increase in packing density at the bottom of the compressing sediment can only be clearly observed via the biexponential fitting method. Calculations of the area under the curves revealed that the total solid concentration obtained via the biexponential fitting was 14.3%, whereas measured volume fractions via the monoexponential and signal intensity methods were 19.6 and 21.5%, respectively.

As it is clear from Figure 2 for this specific system, that using the mono- and biexponential model do not lead to identical systems descriptions, F-tests were performed on a pixel-by-pixel basis over the entire profile, to compare the results obtained by the two fitting methods. Although the values of F_{12} observed for the fluid region following sedimentation given in Figure 3b can be exceeded by about 1% of random observations, Figure 3a shows that the values of F_{12} for the fitted curves of the sediment region are not within the confident intervals. Thus, it is justified to add further terms to the fitting function to describe the signal decay of voxels belonging to the particulate region.

In summary, the mean values and the standard deviations of the particle volume fractions measured over the settled sediment of 15% v/v activated carbon in doped water via the mono- and biexponential models are 0.40 ± 0.03 and 0.54 ± 0.02, respectively. The mean statistic F (F_{12}) in the sediment region is 37 ± 18, and the critical values of F corresponding to the probability of 0.01 of exceeding F range from 0.3 ± 0.1 to 3.2 ± 0.6.

Subsequent to the above, an identical study was performed for the initial projection which was expected to evaluate any homogeneous mixture of particles along the vertical height of the suspension. The mean volume fractions for the mono- and biexponential methods were 0.21 ± 0.01 and 0.15 ± 0.01 along the entire projection; furthermore, $F_{12} = 25 \pm 6$, and the critical limits were 0.40 ± 0.02 and 2.4 ± 0.1, respectively. This implies that the use of the two-term

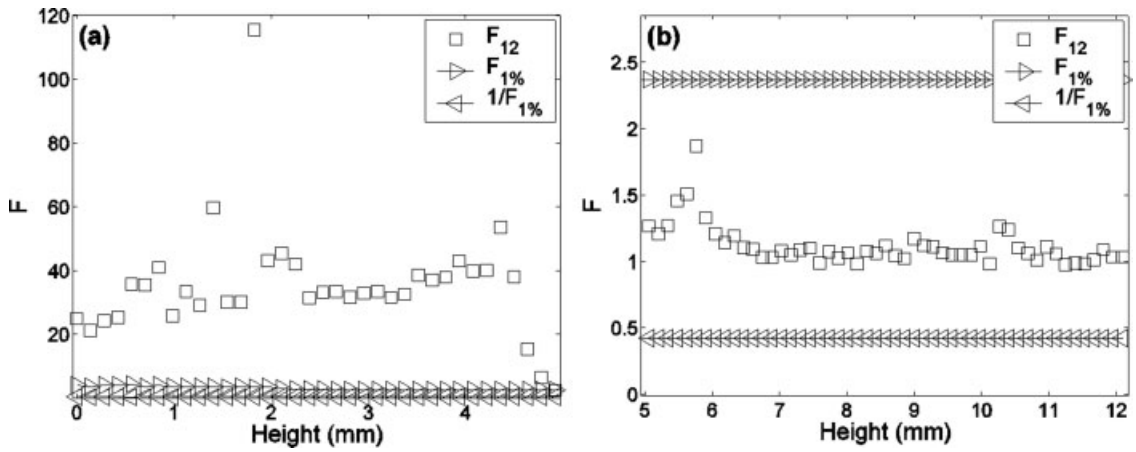

Figure 3. The square symbols in these graphs indicate the value of the statistic F (F_{12}) for the vertical dimension of 15% v/v activated carbon, which has settled from an aqueous CuSO4 (6.3 mM) solution.

The parameters $F_{1\%}$ and $1/F_{1\%}$ characterize the critical values of F, which correspond to the probability of exceeding F, 0.01.

Table 2. Mean Particle Volume Fractions ($\bar{\Phi}$) Calculated via the Mono- and the Biexponential Models, plus the Values of Statistic F (F_{12}) and Critical Ranges of F for the Particulate Region of Different Settled Solids in Doped Water

Solid Phase	Approx. Size (μm)	Initial Solid Concentration (% by vol.)	$\bar{\Phi}_{\text{biexponential}}$	$\bar{\Phi}_{\text{monoexponential}}$	F_{12}	$[1/F_{1\%}\ F_{1\%}]$
Carbon	44–149	15	0.40 ± 0.03	0.54 ± 0.03	37 ± 18	0.33 ± 0.06–3.2 ± 0.6
Talc	9	35	0.63 ± 0.03	0.73 ± 0.03	40 ± 7	0.40 ± 0.02–2.5 ± 0.1
$CaCO_3$	7–10	15	0.43 ± 0.03	0.53 ± 0.02	27 ± 4	0.36 ± 0.05–2.9 ± 0.4
Glass beads*	150	20	0.66 ± 0.01	0.71 ± 0.01	20 ± 5	0.30 ± 0.02–3.5 ± 0.2
Polystyrene beads*	3–17	45	0.61 ± 0.03	0.61 ± 0.03	1.1 ± 0.1	0.42 ± 0.01–2.4 ± 0.1

*Nonanionic surfactant was added to avoid agglomeration of particles.

method is necessary for accurate measurements of particle volume fractions over the complete sedimentation process.

Table 2 summarizes the mean volume fractions and fit test data obtained for the compressible sedimentation of carbon, talc, and $CaCO_3$, plus the incompressible sedimentation of glass beads and of colloidal polystyrene beads. A nonanionic surfactant (0.03% w/w) was added to the glass and polystyrene beads aqueous $CuSO_4$ (6–14 mM) suspensions to suppress aggregation of the particles and ensure a homogeneous formation of the sediment. Data for talc and calcium carbonate are only illustrative; further details of the sedimentation of carbon, talc, $CaCO_3$, three-phase and commercial suspensions using the method proposed here will be reported in a subsequent publication.

It is clear from these results that only the sedimentation of polystyrene beads is compatible with the monoexponential fitting method. This reflects the low magnetic susceptibility difference between the solid and the liquid phases, which means that the field distortions caused by the polystyrene particles are low, and hence that water molecules diffusing in the sediment region do not experience a large range of instantaneous Larmor frequencies.

A further experiment showed that small particles packed more loosely with increase in the viscosity of the fluid; thus, 150-μm glass beads from an aqueous 98% v/v glycerol solution packed at a lower density, $\Phi = 0.58 \pm 0.01$, than from water, $\Phi = 0.66 \pm 0.01$. Note that, although the diameter of the glass beads is larger than the linear resolution of the MRI projection, the volume occupied by one particle is still much smaller than the voxel size; hence, the effects on the MR-signal decay due to the finite encoding along the read direction can be neglected.

Figure 4 represents the relation between particle volume fraction and the T_2 components as a function of height for some of the systems mentioned earlier. Specifically, Figure 4a shows the spatial distribution of T_{21} and T_{22} vs. particle volume fraction for the settled activated carbon suspension. Gradients in T_2 as a function of height found at the bottom of the vessel are consistent with the expectation that larger particles must be located at the bottom of the sedimentation column. This reflects the fact that although field distortion increases with particle volume fraction, at identical solid concentrations the polarizing field perturbation decreases with increase of the particle size.

The structure of the quasi-settled polystyrene bead suspension represented by the data given in Figure 4b can be explained by the same logic, in which nonanionic surfactant causes a very organized settling and packing of the particles. Thus, a vertical gradient of the T_2 values along the height of the sediment indicates a gradient in particle size for approximately constant volume fraction (height 0–6.5 mm); this is a consequence of bigger particles settling faster than smaller colloidal beads. Because particles are anticipated to separate according to particle size during the settling process and monodisperse spheres are always expected to pack at the same volume fraction ($\Phi \approx 0.6$), a reduction in both, packing density and T_2 at the sediment interface (height 6.5–8.5 mm), suggests that some tiny suspended polystyrene beads have not yet settled (the associated cloudy region was visible to the naked eye).

It is clear that the effect of the nonanionic surfactant on the screening of the particle surfaces prevents particle aggregation; in contrast, Figure 4c shows a single profile of a suspension which was initially allowed to pack for 2 days, and was then poorly mixed to maintain the particles conglomerated, forming fragile structures. The figure illustrates an irregularity of the T_{21} profile that can be explained as a consequence of the agglomeration of polystyrene particles at about 1 mm from the bottom of the suspension. Note that flocs consist of both, aggregates of solids and occluded fluid, hence there is a slight increase in volume fraction in that region; also that the increase in the relaxation times, just below and above the agglomeration, is the result of lower magnetic field distortions in those regions, because in terms of magnetic field perturbation, particle agglomerations behave equivalent to large particles. An alternative explanation based on the presence of one or more air bubbles was rejected because of the shape of the T_{21} profile in Figure 4c. Taking the sediment interface as a reference, there are two increases in T_{21} in the particulate region, as opposed to one decrease from the bottom to the top of the sediment, as would be expected if the increase in volume fraction was produced by a void with much higher magnetic susceptibility.

Figure 5 shows the evolution in time both of the particle volume fraction and of the most relevant T_2 component as a function of height for the same suspension illustrated in Figure 4c, namely, a suspension of 19% v/v 3- to 17-μm diameter polystyrene beads settling in an aqueous 8.5 mM $CuSO_4$ solution. It illustrates the potential of this MRI technique to measure some important properties of suspensions, such as the settling rate, the hindered settling function, the interface broadening effects, and the evolution of the sediment, which has been extensively described by Davis and Hassen.[8] However, it is important to note that complementary information can also be obtained from detailed studies of the projections of the measured relaxation times. Figures 5c,d show that the agglomeration previously described was initiated between particles that settled at very early stages of the process ($t \sim$

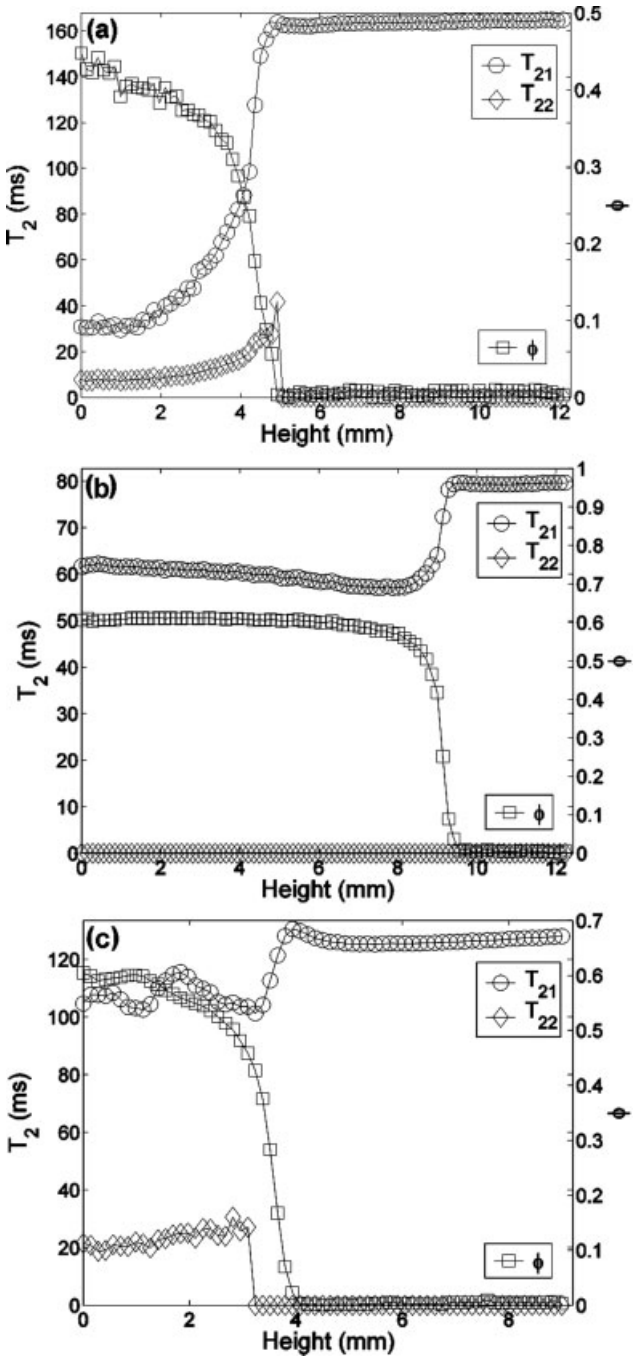

Figure 4. Particle volume fraction and relaxation time components, obtained via biexponential fitting, as a function of time.

For: (a) 15% v/v activated carbon settled from an aqueous 6.3 mM CuSO4 solution; (b) 45% v/v 3- to 17-μm diameter polystyrene beads settled from an 0.3–99.7% w/w TRITON X-100–aqueous 13.5 mM CuSO4 solution; and (c) 19% v/v 3- to 17-μm diameter polystyrene beads settled from an aqueous 8.5 mM CuSO4 solution.

$2'30''$, $T_2 \sim 88$ ms). The subsequent evolution of the relaxation times shows that those agglomerates were disintegrated as the fluid trapped at the bottom of the sediment was pushed upward by the sediment compaction. The basis for this interpretation is the relaxation time increase with time ($t \sim 2'30''$–$55'$, $T_2 \sim 88$–116 ms), and its later decrease ($t \sim 55'$–$340'$, $T_2 \sim 116$–90 ms) at a height of 1 mm from the bottom of the sediment. As mentioned earlier, flocs essentially act as large particles, hence reducing field distortions and allowing the transverse magnetization to decay at a lower rate. As the sediment compaction evolves, the weight of the settled particles fragments the aggregates and releases the trapped fluid; this results in a reduction of spin–spin relaxation times because of smaller interparticle distances. Note that the measurements shown in Figure 4c were extracted from this set of data and correspond to a profile 300 min after the sedimentation process was initiated.

Summary and Conclusions

A CPMG MRI protocol has been used to measure the settling and packing of a range of colloidal or noncolloidal particles from aqueous solutions. Solid fractions for the settling of 15% by volume activated carbon from a suspension in aqueous 6.3 mM $CuSO_4$ solution were obtained by using the signal intensity (first echo) and the initial magnetization corresponding to the single-exponential and biexponential models, respectively; that is, the point at which the fitted monoexponential and biexponential functions cut the ordinate axis. By comparing the volume fraction projections of the settled suspension deduced by each of the three methods, it was found that the packing densities and particle concentration variations were different in the particulate region for all three methods. Pixel-by-pixel F-tests performed to measure the disagreement between the estimated and parent functions for the mono- and biexponential methods, confirmed that the addition of a second exponential term to describe the signal behavior in the sediment region was justified by comparing the F-statistic with the confidence limits corresponding to the probability of 1% of exceeding F. Similar analyses were made for talc, calcium carbonate, glass beads, and polystyrene beads settled in aqueous solutions; discrepancies were found between the two fitting methods, except for the measurements of solid fractions in the sediment of colloidal polystyrene beads.

The fitting method also allowed calculation of the variations of the relaxation times through the depth of the suspensions, which provided valuable information about both the compaction of the structure of the particulate regions and the associated displacement of fluid. Because the relaxation times of the water protons are expected to decrease with increasing particle volume fraction and fluid self-diffusion or decreasing particle size, comparison of the profiles of the relaxation times with those of the volume fraction profiles suggests that the largest activated carbon particles were located at the bottom of the sediment and therefore had settled fastest. Similarly, gravity-driven particle separation was observed for a partially settled suspension of polydisperse, polystyrene beads reflecting the action of a nonanionic surfactant, which had suppressed particle aggregation. This was in marked contrast to the agglomerate of particles of a settled suspension of the same polystyrene beads in the absence of the nonanionic surfactant, which was clearly illustrated by the T_{21} projection.

It was also demonstrated that the time-dependent evolution of particle volume fractions measured by MRI as a function of height within the sediment can be used to measure median settling velocities and interface thicknesses, in

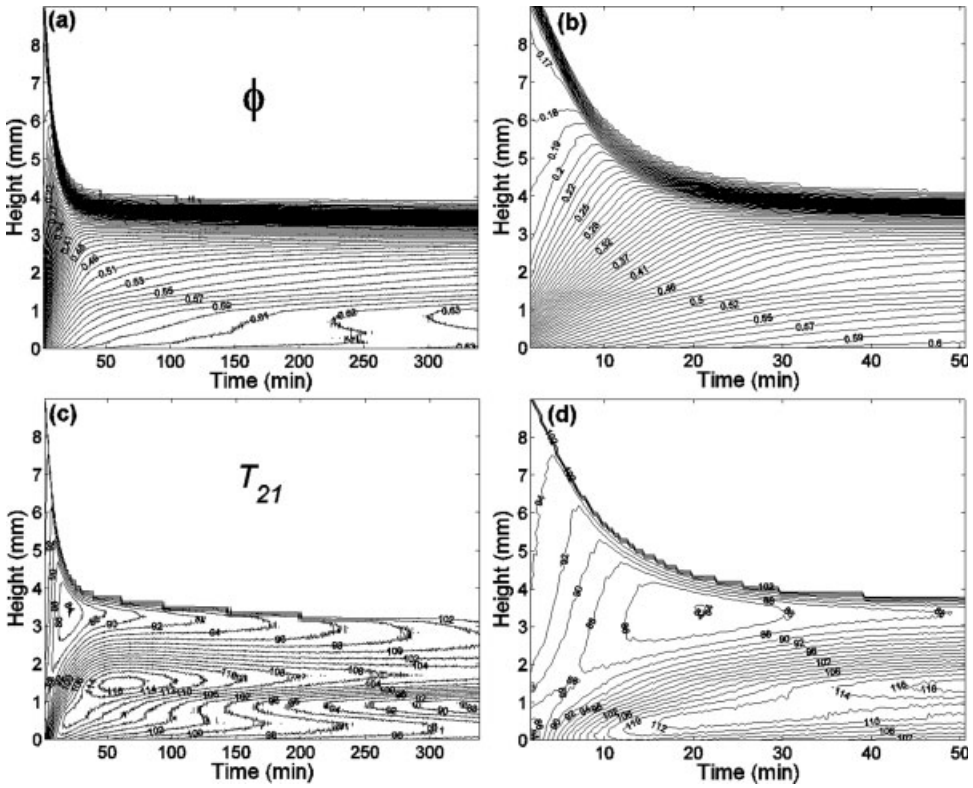

Figure 5. The contour plots in the figure represent 1000 1D (a) volume fraction and (b) T21 profiles as a function of height and time of 19% v/v 3- to 17-μm polystyrene beads settling driven by gravity in an aqueous 8.5 mM CuSO4 solution.

(b) and (d) are zoomed contours from (a) and (c).

confirmation of previous studies.[2,3] However, for the flocculated polystyrene suspension, additional T_2 contour plots allowed a qualitative description of the formation and evolution of the aggregate.

It is appropriate to conclude by reiterating the advantages of using a biexponential model to measure particle volume fractions, and it is hoped that this study will encourage the further use of T_2 data to explore the full potential of the MRI technique to measure settling of multiphase systems.

Acknowledgements

The authors acknowledge the Endowment provided by late Dr. Herchel Smith. They thank Mr. J. P. Valdes-Herrera (Nanoscience Centre, University of Cambridge, U.K.) for providing the micrographs of the particles used in this study.

Literature Cited

1. Lee S, Yang Y, Choi C, Lee T. Combined effect of sedimentation velocity fluctuation and self-sharpening on interface broadening. *Phys Fluids A*. 1992;4:2601–2606.
2. Turney MA, Cheung MK, McCarthy MJ, Powell RL. Magnetic resonance imaging study of sedimenting suspensions of non-colloidal spheres. *Phys Fluids*. 1995;7:904–911.
3. Turney MA, Cheung MK, Powell RL, McCarthy MJ. Hindered settling of rod-like particles measured with magnetic resonance imaging. *AIChE J*. 1995;41:251–257.
4. Chang D, Lee T, Yang Y, Kim M, Lee S. Non-colloidal sedimentation compared with Kynch theory. *Powder Technol*. 1987;92:81–87.
5. Cheung MK, Powell RL, McCarthy MJ. Sedimentation of non-colloidal bidisperse suspensions. *AIChE J*. 1996;42:271–276.
6. Altobelli SA, Mondy LA. Hindered flotation functions from nuclear magnetic resonance imaging. *J Rheol*. 2002;46:1341–1352.
7. Beyea SD, Altobelli SA, Mondy LA. Chemically selective NMR imaging of a 3-component (solid-solid-liquid) sedimenting system. *J Magn Reson*. 2003;161:198–203.
8. Davis RH, Hassen MA. Spreading of the interface at the top of a slightly poly-disperse sedimenting suspension. *J Fluid Mech*. 1988;192:107–134.
9. Hahn EL. Spin echoes. *Phys Rev*. 1950;80:580–594.
10. Muller RN, Gillis P, Moiny F, Roch A. Transverse relaxivity of particulate MRI contrast media: from theories to experiments. *Magn Reson Med*. 1991;22:178–182.
11. Yablonskiy D, Haacke EM. Theory of NMR signal behaviour in magnetically inhomogeneous tissues: the static dephasing regime. *Magn Reson Med*. 1994;32:749–763.
12. Melboom S, Gill D. Modified spin-echo method for measuring nuclear relaxation times. *Rev Sci Instrum*. 1958;29:688–691.
13. Nelder JA, Mead R. A simplex method for function minimization. *Comput J*. 1965;7:308–313.
14. Henkelman RM. Measurements of signal intensities in the presence of noise in MR images. *Med Phys*. 1985;12:232–233.
15. Bevington PR, Robinson DK. *Data Reduction and Error Analysis for the Physical Sciences*, 2nd ed. New York: McGraw-Hill, 1994:194–220.

Manuscript received Nov. 8, 2007, revision received Aug. 21, 2008, and final revision received Oct. 14, 2008.